Acta Biomaterialia 32 (2016) 210–222

Contents lists available at ScienceDirect

Acta Biomaterialia

journal homepage: www.elsevier.com/locate/actabiomat

Full length article

Matrix dimensionality and stiffness cooperatively regulate osteogenesis of mesenchymal stromal cells

Wen-Ting Hsieh [a], Yi-Shiuan Liu [b], Yi-hsuan Lee [c], Marilyn G. Rimando [d], Keng-hui Lin [c,*], Oscar K. Lee [e,f,g,*]

[a] Program in Molecular Medicine, National Yang-Ming University and Academia Sinica, Taipei, Taiwan
[b] Stem Cell Research Center, National Yang-Ming University, Taipei, Taiwan
[c] Institute of Physics, Academia Sinica, Taipei, Taiwan
[d] Taiwan International Graduate Program in Molecular Medicine, National Yang-Ming University and Academia Sinica, Taipei, Taiwan
[e] Taipei City Hospital, Taipei, Taiwan
[f] Institute of Clinical Medicine, National Yang-Ming University, Taipei, Taiwan
[g] Department of Orthopedics and Traumatology, Taipei Veterans General Hospital, Taipei, Taiwan

ARTICLE INFO

Article history:
Received 15 September 2015
Received in revised form 14 December 2015
Accepted 10 January 2016
Available online 11 January 2016

Keywords:
Mesenchymal stromal cells (MSCs)
Matrix stiffness
Osteogenesis
Polyacrylamide scaffold

ABSTRACT

Osteogenic potential of mesenchymal stromal cells (MSCs) is mechanosensitive. It's affected by the mechanical properties of the cellular microenvironment, particularly its mechanical modulus. To explore the effect of mechanical modulus on osteogenesis in the third dimension (3D), this study used a novel polyacrylamide (PA) scaffold whose pores are monodisperse and spherical, the mechanical moduli of which can be tuned across a wide range. It was found that MSCs have similar proliferation rates in PA scaffolds independent of the matrix stiffness. The contractile force exerted by MSCs inside PA scaffolds was strong enough to deform the pores of scaffolds made of more compliant PAs (whose shear modulus, $G'_{scaffold}$ < 4 kPa). Only scaffolds of the highest stiffness ($G'_{scaffold}$ = 12 kPa) can withhold the contraction from MSCs. After osteogenic induction for 21 days, the expression profiles of marker genes showed that PA scaffolds of $G'_{scaffold}$ = 12 kPa promoted osteogenesis of MSCs. Confocal image analysis demonstrated that there are more F-actin cytoskeletons and bundled stress fibers at higher matrix moduli in 2D and 3D. Moreover, the 3D porous structure promotes osteogenesis of MSCs more than 2D flat substrates. Together, the differences of cellular behaviors when cultured in 2D and 3D systems are evident. The PA scaffolds developed in the present study can be used for further investigation into the mechanism of MSC mechanosensing in the 3D context.

Statement of Significance

Mechanical properties of the microenvironment affect cellular behaviors, such as matrix stiffness. Traditionally, cell biological investigations have mostly employed cells growing on 2D substrates. The 3D porous PA scaffolds with the same topological conformation and pore sizes but different stiffness generated in this study showed that the differences of cellular behaviors in 2D and 3D systems are evident. Our 3D scaffolds provide insights into tissue engineering when stem cells incorporated with 3D scaffolds and support the future studies of cellular mechanobiology as well as the elucidation the role mechanical factor plays on the physiology and fate determination of MSCs in the 3D context.

1. Introduction

Stem cells sense and respond to complex biochemical and physical signals from their extracellular microenvironment niche, which controls stem cell lineage specification [1,2]. Understanding the interactions between cells and their microenvironment is the key to enabling successful stem cell-based therapy and regenerative medicine. While much attention has been focused on biochemical signals, recent evidence has indicated that physical signals play an equally important role, also known as mechanotransduction. It is evident that bone regeneration involves mechanotransduction because bones constantly adapt to external loading and go through remodeling with physical exercise, which

* Corresponding authors at: Taipei City Hospital, No. 145, Zhengzhou Road, Datong District, Taipei 10341, Taiwan (O.K. Lee). Institute of Physics, Academia Sinica, No. 128, Section 2, Academia Road, Nankang District, Taipei 11529, Taiwan (K. Lin).

E-mail addresses: khlin@phys.sinica.edu.tw (K.-h. Lin), DAV47@tpech.gov.tw (O.K. Lee).

http://dx.doi.org/10.1016/j.actbio.2016.01.010
1742-7061/

exerts loads on bones and increase bone density [3–5]. Identifying the physical signals induce osteogenesis of mesenchymal stromal cells (MSCs) is important for both fundamental understanding and clinical translation of skeletal tissue engineering [6].

The most-studied physical signal for mechanotransduction is the mechanical modulus of the matrix, which directs MSCs into osteoblasts at high stiffness [7] through α2-integrin mediated signaling pathways including Rho/ROCK, FAK, and ERK1/2 [8]. Recent findings directly link the rigidity sensing to the nuclear transcriptional factors YAP/TAZ involved the canonical Hippo signaling pathway [9]. These findings demonstrate that matrix stiffness is a key regulator in controlling the osteogenic potential of MSCs but are often demonstrated on two-dimensional (2D) compliant substrates made of polyacrylamide (PA) [7–9].

A three-dimensional (3D) culture scaffold provides more architectural and material diversity than a 2D substrate and recapitulates the *in vivo* microenvironment. The direct application of a 3D scaffold is tissue regeneration. Nevertheless, a handful of studies have investigated the impact of 3D matrix stiffness on MSC differentiation [10–14]. One major challenge in controlling 3D matrix stiffness is to decouple biochemical factors, which cannot be achieved by reconstituting the ECM culture, because the ECM provides both mechanical and biochemical signals to cells and thus confounds data interpretation. This limit can be overcome by independently conjugating adhesive ligands on non-adhesive synthetic or natural polymers such as polyethylene glycol (PEG) or alginate. Huebsch et al. generated 3D alginate matrices with different rigidities (2.5–110 kPa) covalently linked to a synthetic ECM containing RGD (Arg–Gly–Asp). They demonstrated that the osteogenic commitment of clonally derived murine MSCs occurred predominantly at 11–30 kPa [10]. Pek et al. cultured MSCs in thixotropic gels with varying rigidity in 3D and demonstrated that the expressions of neural (ENO2), myogenic (MYOG) and osteogenic (Runx2, OC) transcription factors were highest for gels with respective liquefaction stresses of 7, 25 and 75 Pa [11]. Both work provided insights to develop a culture scaffold independently control mechanical and biochemical cues to the cells. However, both works entrap MSCs inside a polymer matrix and thus restrict the MSC morphology into a grossly spherical shape. A micro-porous scaffold allows cells to spread, migrate, and form cell–cell contact without restriction, which is important for bone tissue engineering.

A different scheme to fabricate 3D scaffolds with tunable stiffness is to produce commonly used PA substrates with 3D characteristics by making the substrate negatively curved. Lee et al. demonstrated the fabrication of a 3D PA porous scaffold, where fibroblasts in the scaffold sensed local stiffness and dorsal–ventral asymmetry is lost as *in vivo* [15]. In this study, the PA porous scaffolds with controlled curvatures whose radii of curvature were between 50 and 60 μm (or equivalently pore sizes between 100 and 120 μm) and different scaffold stiffness values (Group I–III, 1, 4 and 12 kPa) were fabricated. The porosity of the PA scaffolds (70%) resembles the range of porosity of trabecular bones (50–90%) [15,16]. Tunable stiffness and pore size help simplify the complexity of existing 3D cultured platforms. The 2D PA substrates of corresponding stiffness (Group IV–VIII, 1, 5, 11, 55 and 121 kPa) were performed as control. Cell morphology, F-actin organization, proliferation, viability, and osteogenic potential between the 2D and 3D microenvironments were compared. The purpose of this study is to examine how matrix dimensionality and stiffness determine the osteogenic fate of MSCs through mechanotransduction events both in 2D and 3D culture systems. A hypothesis is thus proposed that 3D PA scaffolds with different stiffness regulate osteogenesis of MSCs via the organization of F-actin cytoskeletons.

2. Methods

2.1. Cell culture and osteogenic differentiation of MSCs

Commercially available human MSCs were used in this study (Steminent Biotherapeutics, Inc. Taipei, Taiwan, passage number = 8). MSCs were maintained in the growth medium consisting of Iscove's Modified Dulbecco's medium (IMDM; Invitrogen) and 10% fetal bovine serum (Sigma–Aldrich), 10 ng/ml basic fibroblast growth factor (Sigma–Aldrich), 100 units of penicillin, 1000 units of streptomycin, and 2 mM L-glutamine (Sigma–Aldrich). For osteogenic differentiation experiments, MSCs (passage number = 10) were seeded into 3D PA scaffolds and on 2D PA substrates and maintained in the growth medium for 48 hours. The MSCs were then treated with osteogenic induction medium for 21 days and osteogenic induction medium was changed twice a week. The day before shifting to osteogenic induction medium was defined as day 0. The osteogenic induction medium consisted of IMDM supplemented with 0.1 μM dexamethasone (Sigma–Aldrich), 10 mM beta-glycerol phosphate (Sigma–Aldrich), and 0.2 mM ascorbic acid (Sigma–Aldrich). The seeding density of the MSCs was 10^5 cells per 3D PA scaffold and 4000 cells/cm^2 per 2D PA hydrogel.

2.2. Fabrication of polyacrylamide scaffolds and hydrogels

PA scaffolds were prepared following the method described in Lee et al. [15]. Briefly, a polydimethylsiloxane-based microfluidic device consisting of three inlets and one outlet channel was used to generate monodisperse foam (Fig. 1A). A PA precursor solution containing acrylamide (AC, Bio-rad), bis-acrylamide (BIS, crosslinker, Bio-rad), Pluronic® F-127 (surfactant, Sigma-Aldrich), and N,N,N′,N′-tetramethylethylenediamine (TEMED, catalyst, Sigma–Aldrich) was passed to one inlet and passed nitrogen air saturated with perfluorohexane (C_6F_{14}) to another inlet channel. The liquid channel was subsequently split into two symmetric channels and then merged with the air channel at the cross junction where the air stream was squeezed by two opposite liquid streams and broken up into a uniform bubble train toward the outlet channel. The initiator, 1% ammonium persulfate (APS, Sigma–Aldrich) solution, was injected into the foam stream from the third inlet channel at the downstream of the cross junction to mix with the PA precursor solution to initiate the gelling. The downstream output channel was designed in a serpentine shape to facilitate the mixing of the initiator with the PA precursor solution. The well-mixed PA foam solution was collected at the outlet channel into a disk reservoir 6 mm in diameter and 1 mm in height. The filled reservoirs were placed in an oven at 80 °C for 2 min to immediately solidify the foam. The solid foam was further placed in a vacuum chamber to be opened for subsequent treatment.

For the cell culture, the surface of both PA scaffolds and hydrogels were activated with 1 mg/ml sulfosuccinimidyl 6-(4′-azido-2′-nitrophenylamino) hexanoate (Sulfo-SANPAH, Thermo) for 8 min under UV light (UVP, CL-1000) and then conjugated with 0.5 mg/ml fibronectin (Sigma–Aldrich) for 2 h at room temperature. Three AC/BIS concentrations (referred as Group I–III in Table 1) were used to fabricate scaffolds of different degrees of stiffness. 2D PA substrates were made using a polyacrylamide precursor solution and a gelling agent between two square glass plates with a spacer of 36 cm^2 in area and 750 μm in height. Five AC/BIS concentrations (referred as Group IV–VIII in Table 1) were used for the experiment to cover the range of stiffness similar to that of the scaffold and gel (Table 1, Group I–VIII).

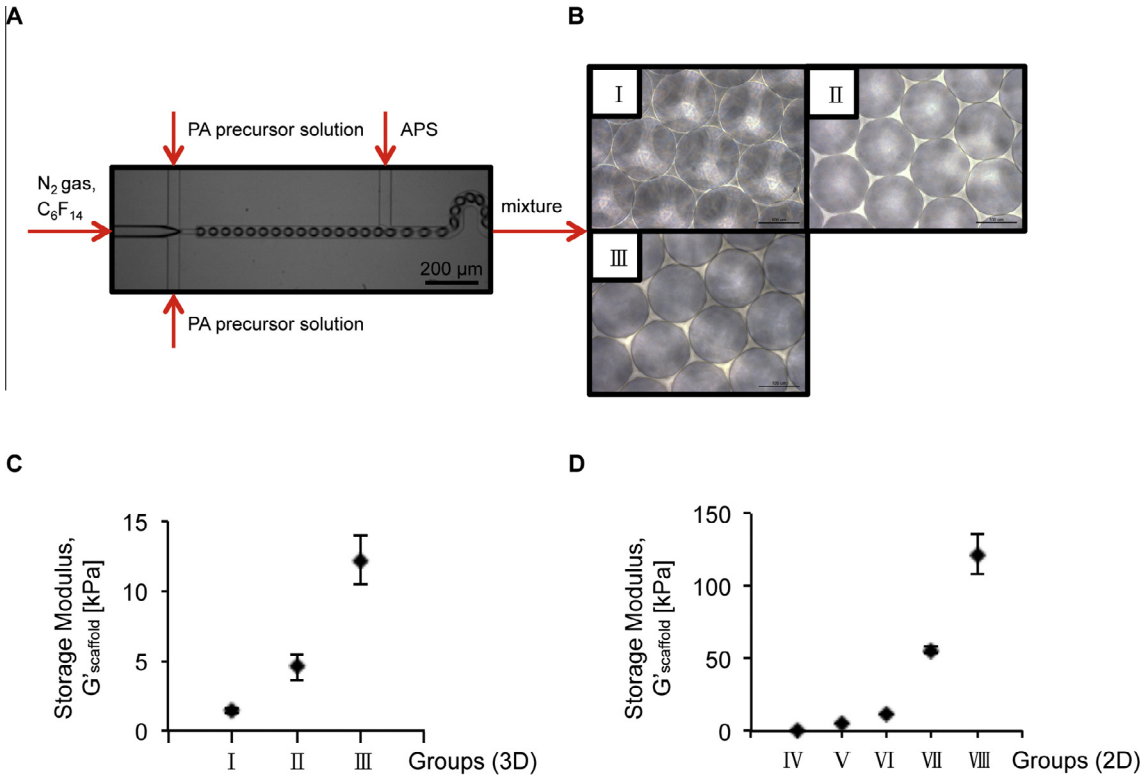

Fig. 1. Fabrication and characterization of the 3D polyacrylamide (PA) scaffold (A) microfluidic device was designed to fabricate PA scaffold. Scale bar = 200 μm. (B) The pore size of 3D PA scaffold (Groups I–III) was identical 100–120 μm. Scale bar = 100 μm. (C) The shear storage moduli ($G'_{scaffold}$) of Groups I–III was 1 ± 0.16 kPa, 4 ± 0.98 kPa and 12 ± 1.73 kPa, respectively (data represented mean ± S.D., n = 10, ten scaffolds were analyzed for each group). (D) The shear storage moduli (G'_{gel}) of Groups IV–VIII was 1 ± 0.15 kPa, 5 ± 0.33 kPa, 11 ± 0.61 kPa, 55 ± 2.13 kPa and 121 ± 14 kPa, respectively (data represented mean ± S.D., n = 10, ten hydrogels were analyzed for each group).

Table 1
Composition and physical properties of PA scaffolds and hydrogels. The stiffness of 3D scaffolds and 2D substrates was measured by rheometer. The storage modulus (G') represented mean ± S.D., n = 10 (ten scaffolds and hydrogels were analyzed for each group). The gene expression profiles between 3D scaffolds and 2D substrates were analyzed by similar overall stiffness (i.e. Group I vs. Group IV, II vs. V, III vs. VI) and the same concentration of AC/BIS (i.e. Group I vs. V with a horizontal stripe pattern, II vs. VII with a vertical stripe pattern, and III vs. VIII with a grid pattern). TEMED; N,N,N′,N′-tetramethylethylenediamine, APS; ammonium persulfate, F-127; Pluronic® F-127.

Dimensionality	3D	3D	3D	2D	2D	2D	2D	2D
Group	I	II	III	IV	V	VI	VII	VIII
Acrylamide (%)	7	12	18.75	5	7	12	12	18.75
Bis-acrylamide (%)	0.2	0.6	1.13	0.1	0.2	0.145	0.6	1.13
TEMED, APS, F-127 (%)	1	1	1	1	1	1	1	1
Pore size (μm)	100 ± 20	100 ± 20	100 ± 20					
Storage modulus, G' (kPa)	1 ± 0.16	4 ± 0.98	12 ± 1.73	1 ± 0.15	5 ± 0.33	11 ± 0.61	55 ± 2.13	121 ± 14.14

2.3. Measurement of stiffness of scaffolds and hydrogels

The stiffness of the PA scaffolds and homogenous gels was measured by detecting the storage moduli ($G'_{scaffold}$ and G'_{gel}). PA scaffolds and gels were soaked for 24 h until completely swollen before measurement. The measurement was carried out by rheometer (Physica MCR 301, Anton Paar) using a disposable parallel plate holder (diameter 25 mm, D-CP/PP7, Anton Paar) subjected to oscillatory shear with a maximum strain of 0.005% at 1 Hz. The storage modulus ($G'_{scaffold}$ and G'_{gel}) represented mean ± S.D., n = 10 (ten scaffolds and hydrogels were analyzed for each group).

2.4. Circularity measurement of pore of PA scaffolds

To measure the deformation of a spherical pore, the circularity C of pore was defined as

$$C = 4\pi A/P^2$$

where A is the area and P is the perimeter [17]. The maximum value of C is 1 for a circle and it decreases as the shape deviates from a circle. ImageJ was used to outline the shape of pores based on bright-field images and calculated the area and perimeter of the selected pores (n = 20, Group I–III) at each time points.

2.5. Cell proliferation assay

The proliferation rate and viability of the MSCs adhered to the PA scaffolds was assessed by CellTiter 96® Aqueous One Solution Cell Proliferation Assay (Promega). The reagent contains a tetrazolium compound (3-[4,5-dimethythiazol-2-yl]-5-[3-carboxy-methoxyphenyl]-2-[4-sul-fophenyl]-2H-tetrazolium, inner salt, MTS) and an electron coupling reagent (phenazine ethosulfate, PES). MSCs in the PA scaffolds were incubated with CellTiter reagent and culture medium in the dark at 37 °C for 1 h. The absorbance at an optical density (OD) of 490 nm was measured for the assessment of viable MSCs. The proliferation rate was analyzed after

seeding MSCs into the PA scaffolds 1, 7, 14 and 21 days. Data represented mean ± S.D., $n = 3$ (three independent experiments).

2.6. RNA extraction and real-time qPCR

MSCs were cultured in 3D PA scaffolds and 2D PA substrates. Each PA scaffold and hydrogel was washed with 1× PBS for three times. Total RNA then extracted according to the RNeasy® Mini Kit Spin Protocol (QIAGEN). The integrity of the RNA extracts were checked by 1.2% (w/v) agarose gel electrophoresis and the concentration of RNA were quantified using OD 260/280. After extraction, RNA was reverse transcribed to cDNA by MMLV reverse transcriptase (EPICENTRE® Biotechnologies). Specific primers for different osteogenic marker genes were designed using the Universal Probe Library System (Roche Applied Science) to detect gene expression in MSCs that were adhered to PA scaffolds and hydrogels with different degrees of stiffness (Table A.1). All the reactions were performed on the StepOnePlus Real-Time PCR System. The average threshold cycle for each marker gene was normalized by glyceraldehyde 3-phosphate dehydrogenase (GAPDH). Gene expression of 3D scaffolds and 2D substrates were analyzed by similar overall stiffness (i.e. Group I vs. Group IV, II vs. V, III vs. VI) and the same concentration of AC/BIS (i.e. Group I vs. V with a horizontal stripe pattern, II vs. VII with a vertical stripe pattern, and III vs. VIII with a grid pattern). All data represented mean ± S.D., $n = 3$ (three independent experiments).

2.7. Immunofluorescence staining and quantification of images

After inducing osteogenic differentiation of MSCs for 24 h, non-adherent MSCs were removed by PBS washing. The MSCs in the 3D PA scaffolds and 2D PA hydrogels were fixed in 4% paraformaldehyde (Sigma–Aldrich) for 30 min, and permeabilized with 0.5% Triton X-100 in PBS for 10 min. The fixed MSCs were stained with 6.6 μM rhodamine phalloidin (Life Technologies) and 10 μg/ml DAPI (Santa Cruz Biotechnology) in PBS for 30 min and 10 min, respectively. The visualization of F-actin and nuclei of MSCs in 2D hydrogels and 3D PA scaffolds was carried out with a 20×/0.8 NA air objective or 40×/1.4 NA oil objective on a Zeiss LSM 700 confocal microscope. ZEN (blue and black edition) software from ZEISS was used to analyze the 2D and 3D reconstructive images obtained using the confocal microscope. The immunofluorescence intensity of F-actin of MSCs was quantified using MetaMorph software. The average cytoplasm immunofluorescence intensity from 50 different cells was respectively derived from *z*-stacks of confocal images (depth intervals = 0.5 μm) of a whole cell in 3D PA scaffolds and 2D PA hydrogels (mean ± S.D., $n = 50$).

2.8. Statistical analysis

Microsoft Excel was used to perform Student's *t*-test and the symbol (*) represented statistical significant difference at $p < 0.05$ between different two groups (Fig. 2C and D). IBM SPSS Statistics 19 was used to perform Kruskal–Wallis test followed by Dunn-Bonferroni post hoc test (Figs. 3–5) and one-way ANOVA followed by Tukey's post hoc test (Fig. 6C and D), where different letters (a, b, c, d, e) represented statistically significant difference at 95% confidence intervals between different time points (Figs. 3 and 4) or experimental groups (Figs. 5 and 6). For instance, the expression of Runx2 showed no statistical difference on day 0, 1 and 7 (marked by "a", Fig. 3A, Group I). Expression of Runx2 showed no statistical difference on day 1, 7 and 14 (marked by "b", Fig. 3A, Group I). Expression of Runx2 showed no statistical difference on day 7, 14 and 21 (marked by "c", Fig. 3A, Group I). Expression of Runx2 showed statistically significant difference between day 0, 1 (marked by "a" and "ab", Fig. 3A, Group I) and day 21 (marked by "c", Fig. 3A, Group I).

3. Results

3.1. Characterization of three-dimensional porous polyacrylamide scaffolds

The pore sizes for this study measured between 100 and 120 μm in diameter (Fig. 1B, Group I–III). The storage moduli ($G'_{scaffold}$) of the three PA scaffolds (Table 1, Group I–III) were 1 ± 0.16 kPa, 4 ± 0.98 kPa and 12 ± 1.73 kPa, respectively (Fig. 1C). The storage moduli (G'_{gel}) of the five uniform gels (Table 1, Group IV–VIII) were 1 ± 0.15 kPa, 5 ± 0.33 kPa, 11 ± 0.61 kPa, 55 ± 2.13 kPa and 121 ± 14 kPa, respectively (Fig. 1D). The $G'_{scaffold}$ value of Group I–III is close to that of G'_{gel} of Group IV–VI. For the same AC/BIS concentration, $G'_{scaffold}$ is generally one order less than G'_{gel} (i.e. Group I vs. V, II vs. VII and III vs. VIII). The results were consistent with previous findings [15] and demonstrated that the stiffness of the walls in PA scaffolds was close to those of the corresponding uniform hydrogels.

3.2. Effects of matrix stiffness on proliferation and morphology of MSCs in the 3D scaffolds

To investigate the effects of matrix stiffness on MSC growth in the 3D microenvironment, MSCs were seeded in PA scaffolds from Groups I–III and were maintained in the growth medium up to 21 days. It was observed that MSCs grew across the pores and formed connections between MSCs at the neighboring pores regardless of scaffold stiffness (Fig. 2A, black arrow). A single MSC tended to form multiple protrusions in a pore and multiple MSCs are distributed evenly in the pores of the Group I scaffolds (Fig. 2A, left row). In contrast, a single MSC in the Group II and III scaffolds tended to form a spindle-like bipolar morphology in a pore and multiple MSCs aggregate at the center of pores (Fig. 2A, middle and right rows). Pore deformation of Group I and II PA scaffolds was clearly observed after 21 days of MSC culturing (Fig. 2B, red arrow), but not in the Group III at any time. The circularity of the pores in the PA scaffolds of Group I–III at each time point is shown in Fig. 2C. The circularity of Group I decreased over time and dropped most significantly. The circularity of Group II was maintained at a high value close to 1 in the beginning and dropped significantly on day 21. Interestingly, when MSCs undergo osteogenesis, no deformation of the scaffolds is observed in all three Groups (Fig. A.1). There were fewer cells when MSCs were differentiating and the overall contractile force exerted by MSCs was insufficient to deform the pores. Because the cells exhibit similar proliferation rates in the three groups up to 21 days (Fig. 2D), it is speculated that after a longer period of culturing time without a differentiation medium, increased number of MSCs exert a stronger traction force and deform the pores of Group I and II.

The proliferation rate and viability of MSCs in the 3D PA scaffolds was measured by absorbance at an optical density (OD) of 490 nm. For all three groups, absorbance in the 3D PA scaffolds significantly increased with time (Fig. 2D) and there were no statistical difference among the three groups. Although MSCs exhibits different morphologies under different stiffness values, their proliferation rate and viability were not affected by matrix stiffness up to 21 days of observation.

3.3. Osteogenic marker expressions of MSCs affected by matrix stiffness

Osteogenic differentiation of MSCs is a gradual process from early-stage osteoprogenitors, preosteoblasts, immature and

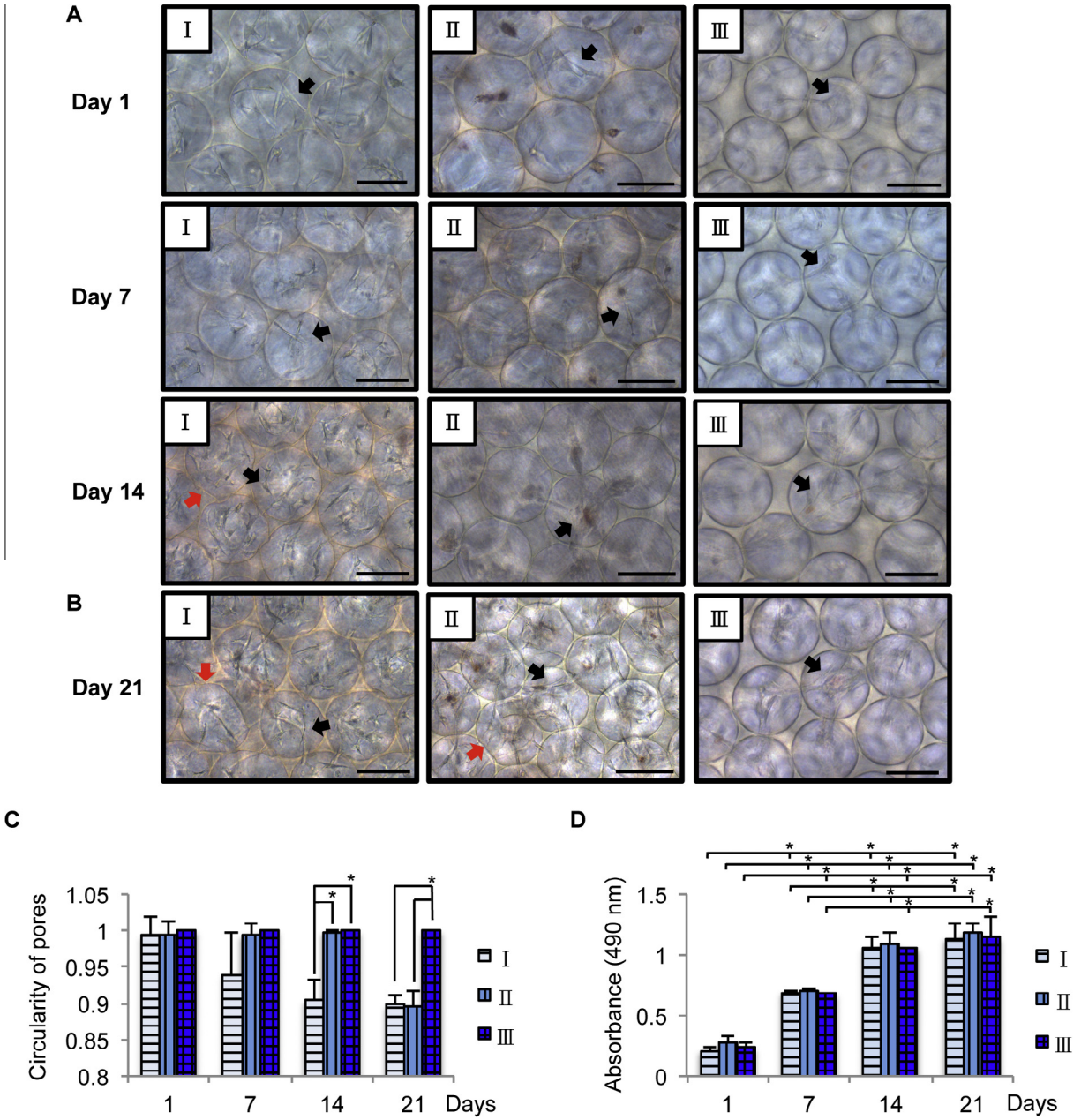

Fig. 2. Cell morphology of MSCs was observed in the (A) Groups I, II and III PA scaffolds after 1, 7, 14 days of culturing (marked by black arrow). Scale bar = 100 μm. (B) The deformation of Group I and Group II was noted after seeding of MSCs for 21 days (marked by red arrow). Scale bar = 100 μm. (C) Circularity measurement of pores of PA scaffolds indicated that Groups I and II showed severe deformation at day 21. Statistical comparison was conducted between the two groups by Student *t*-test and the symbol (*) represents statistical difference, $p < 0.05$. Data represented mean ± S.D., $n = 20$. (D) Proliferation rate of MSCs significantly increased, but there was no significant difference in the three scaffolds at each time point. Data represented mean ± S.D., $n = 3$ (three independent experiments).

mature osteoblasts to late-stage osteocytes. The molecular markers Runx2, osterix, type I collagen, alkaline phosphatase (ALKP) and osteocalcin were used to identify the process. Runx2 directs MSCs into an osteoblastic lineage to become preosteoblasts [18]. Both Runx2 and its downstream osterix further direct preosteoblasts into immature osteoblasts, which produce bone matrix proteins such as type I collagen [19–21]. Type I collagen is highly expressed in osteoblastic cells at all development stages [22]. During osteogenesis, MSCs activate ALKP to mineral deposition. In the mature stage, there is a subsequent decrease in ALKP activity and an increased expression of osteocalcin, which is a later stage marker [23–25]. These osteogenic-related genes, including Runx2, osterix, type I collagen, ALKP and osteocalcin expressions were measured to assess the osteogenic potential in the 3D scaffold.

MSCs in the scaffolds (Group I–III) were induced by osteogenic induction medium for up to 21 days and the expression levels of marker genes were measured on days 0, 1, 7, 14, and 21 by qPCR and normalized to day 0. The expression of Runx2, osterix and type I collagen steadily increases over 21 days after induction for all three groups with the only exception being that Runx2 dropped after 21 days for Group III (Fig. 3A–C). The decrease of Runx2 in Group III suggested osteoblast maturation which would otherwise be inhibited by Runx2 [18]. The expression of ALKP was high up to day 7 and dramatically decreased on days 14 and 21 for all three groups (Fig. 3D). The expression of osteocalcin was also

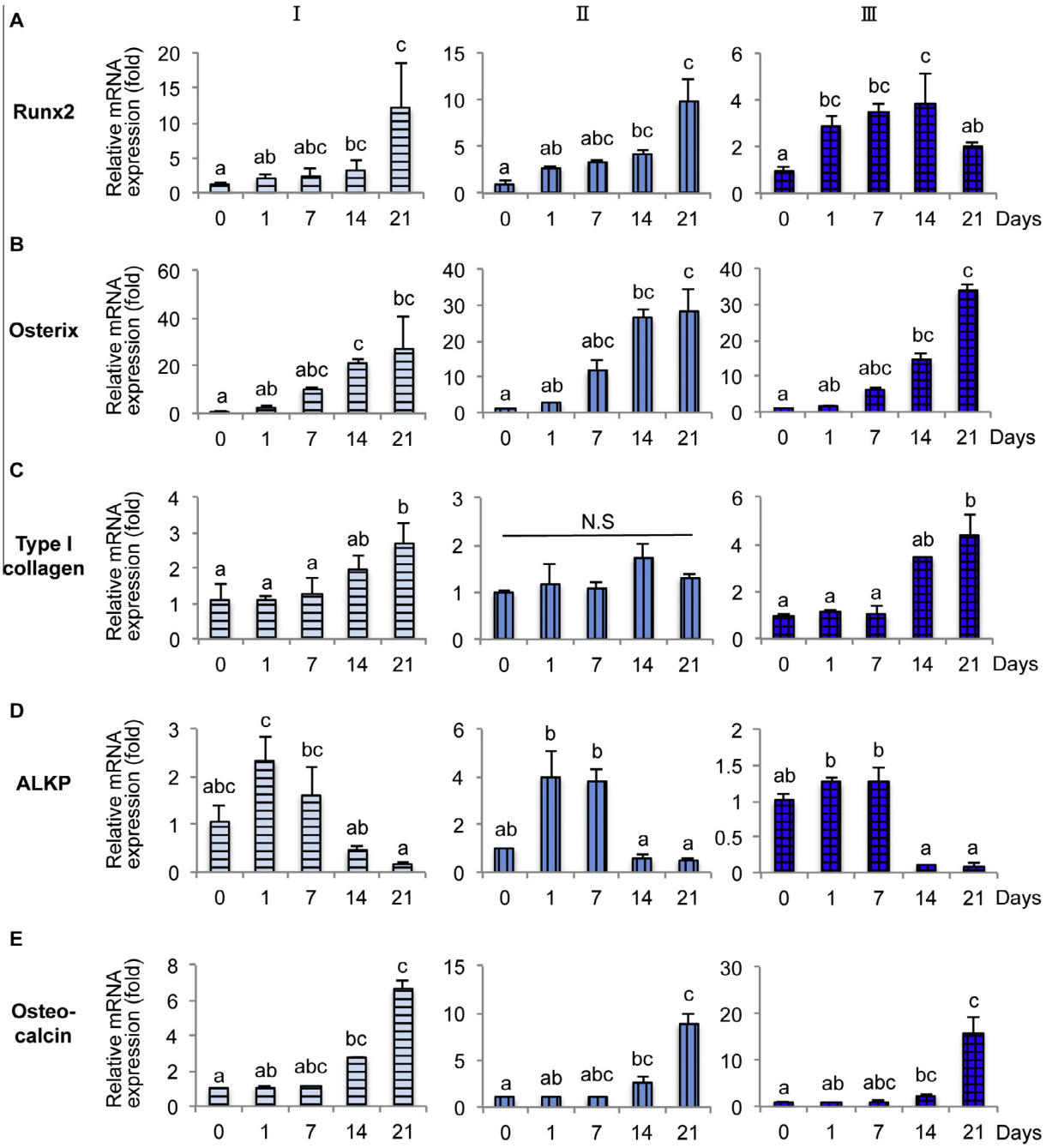

Fig. 3. Gene expression profiles of MSCs during osteogenesis in 3D PA scaffolds (A) relative gene expression of Runx2, (B) osterix, (C) type I collagen, (D) ALKP and (E) osteocalcin in the 3D PA scaffolds (Groups I–III) were measured after inducing osteogenesis for 21 days. Statistical comparison was conducted between multiple groups by Kruskal–Wallis test followed by Dunn-Bonferroni post hoc test and groups with different letters represent statistical difference, $p < 0.05$. Data represented mean ± S.D., $n = 3$ (three independent experiments).

significantly increased on day 21 for all three groups (Fig. 3E). Our results demonstrated that MSCs in the 3D PA scaffolds undergo osteogenesis and increased stiffness directed MSCs into mature osteoblasts.

The same osteogenic marker expressions over time were measured on 2D PA substrates (Group IV–VIII) as controls. The expressions of Runx2 and osterix showed a similar increasing trend over time for all five groups (Fig. 4A and B). The expression of type I collagen showed no statistical difference for four groups (Group IV–VII), and increased expression of type I collagen was only observed on day 21 in the stiffest Group VIII (Fig. 4C). The expression of ALKP in Groups IV, V and VII showed no statistical difference. The expression of ALKP in Group VI increased on day 7 and decreased on day 21. Also, the expression of ALKP increased on day 7 and decreased on day 21 in the stiffest Group VIII (Fig. 4D). The expression levels of osteocalcin for all five groups were significantly increased on day 21 (Fig. 4E). Our results also demonstrated that MSCs on the 2D PA substrates undergo osteogenesis and prefer higher stiffness.

3.4. Effects of matrix stiffness and dimensionality on osteogenic differentiation

To compare the effect of stiffness in both 3D and 2D on osteogenic differentiation, the gene expression was normalized to Group I at each time point. The day before shifting to osteogenic medium

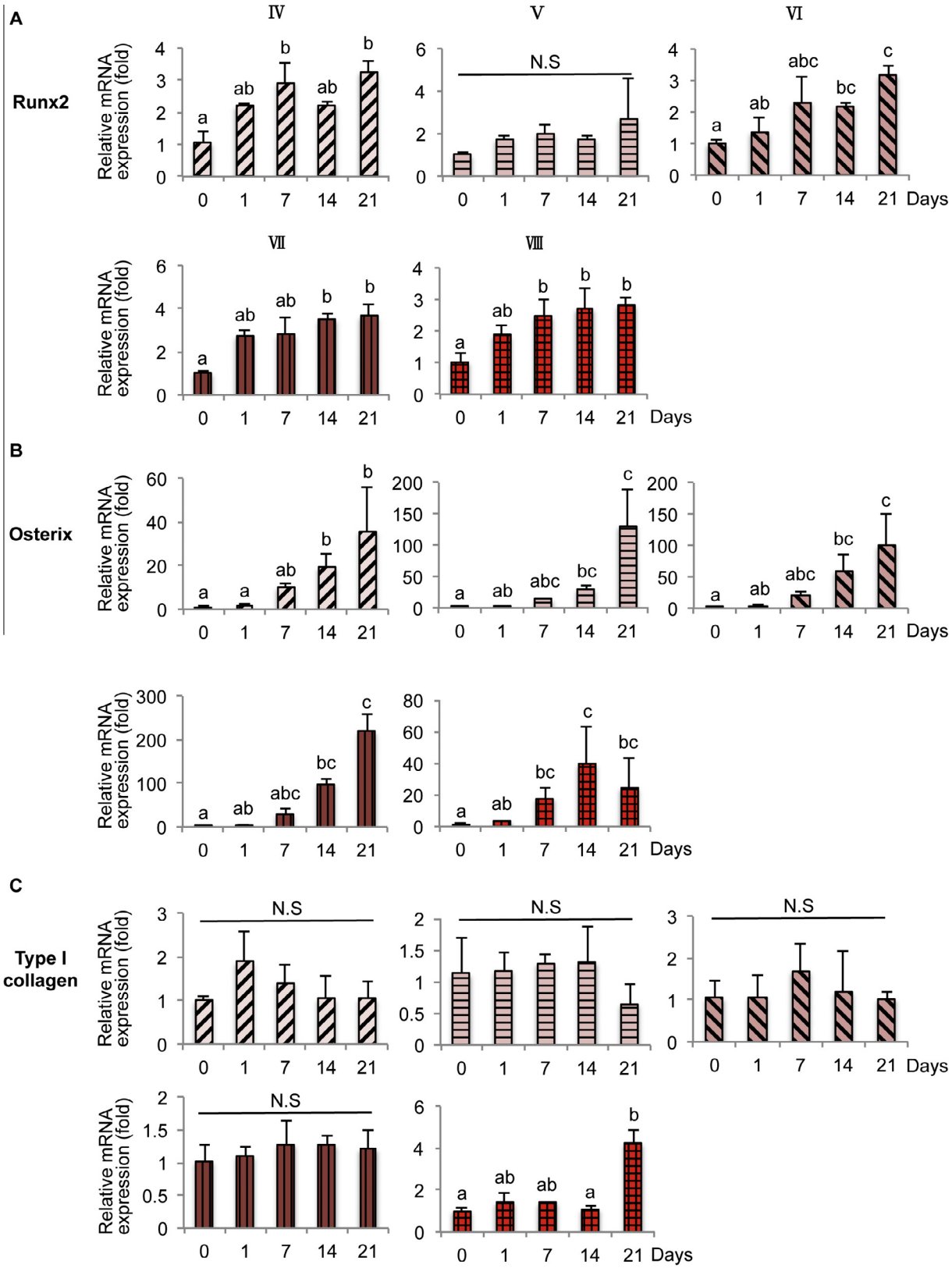

Fig. 4. Gene expression profiles of MSCs during osteogenesis in 2D PA hydrogels (A) relative gene expression of Runx2, (B) osterix, (C) type I collagen, (D) ALKP and (E) osteocalcin in the 2D PA hydrogels (Groups IV–VIII) were measured after inducing osteogenesis for 21 days. Statistical comparison was conducted between multiple groups by Kruskal–Wallis test followed by Dunn-Bonferroni post hoc test and groups with different letters represent statistical difference, $p < 0.05$. N.S = non significant. Data represented mean ± S.D., $n = 3$ (three independent experiments).

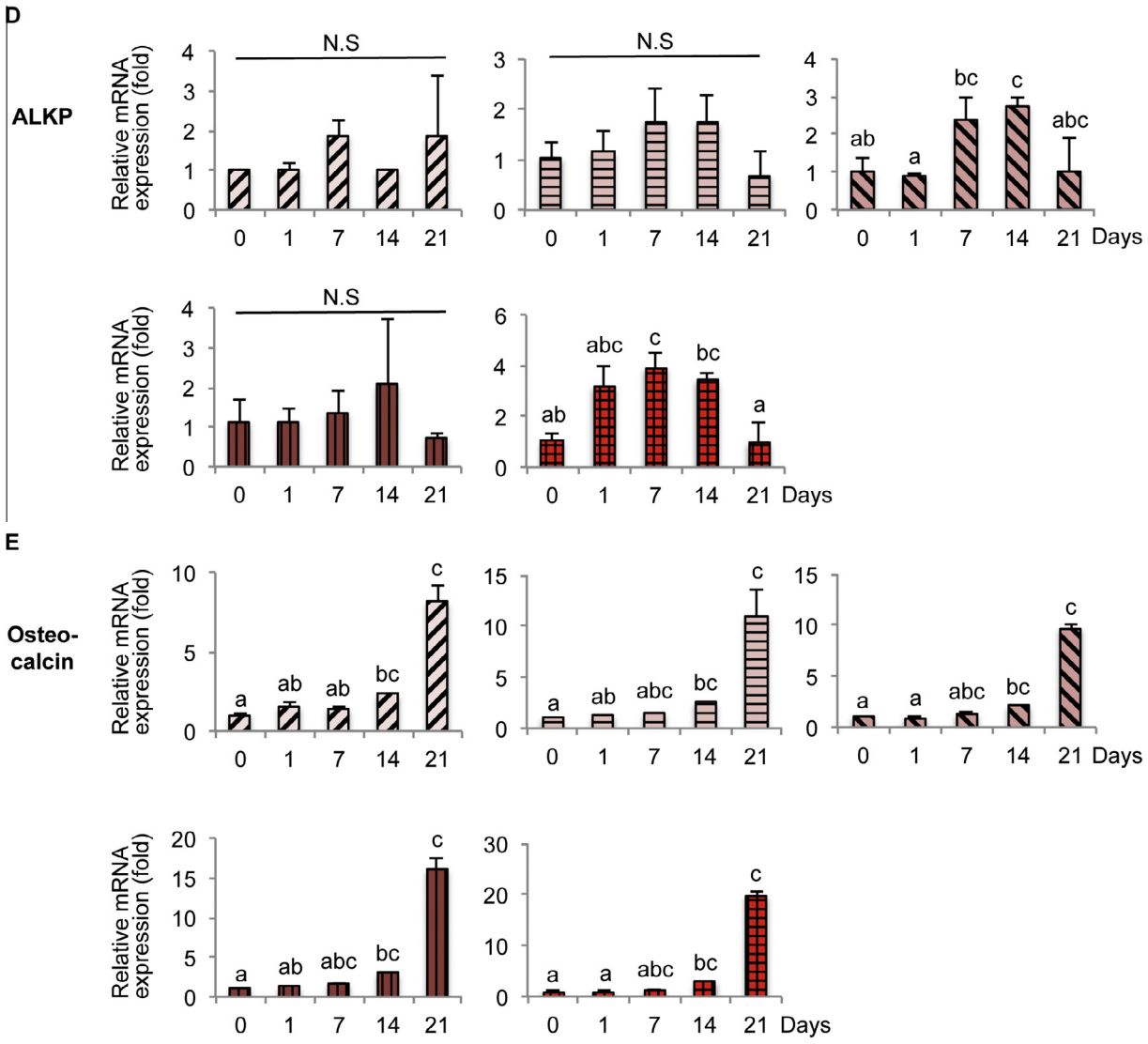

Fig. 4 (*continued*)

was defined as day 0. For 3D scaffolds (Groups I–III) on day 0, the expression of Runx2 and osteocalcin showed no significant increase. However, the expressions of osterix, type I collagen and ALKP in Group III were higher than Group I and II (Fig. 5, blue bars). On 2D substrates (Groups IV–VIII) on day 0, the expression of these osteogenic marker genes showed a trend similar that that of groups with higher stiffness representing higher gene expression levels (Fig. 5, red bars). Different expression level of these osteogenic marker genes on day 0 showed that matrix stiffness impacted MSCs differentiation in 3D and 2D microenvironment occurred without biochemical induction. Even without the biochemical induction, high stiffness and three-dimensionality increase the expression of osteogenic marker genes and cause MSCs to undergo osteogenesis. After inducing osteogenesis, the expression of Runx2 on 3D scaffolds (Groups I–III) increased on day 7 but decreased on day 21 as the stiffness increased (Fig. 5A, blue bars). Osterix expression increased on day 7 and 21 and the levels of Group III were consistently higher than other groups (Fig. 5B, blue bar). Type I collagen expression increased throughout 21 days as the stiffness increased (Figs. 5C, blue bars). The expression level of ALKP on the stiffest Group III was highest on day 7 and lowest on day 14 (Fig. 5D, blue bars). The results indicate that highest stiffness of PA scaffolds promoted maturation of MSCs. The expression of osteocalcin showed no significant difference in all three groups for 21 days (Fig. 5E, blue bars). These results demonstrate that increasing stiffness in the 3D scaffold promotes osteogenic differentiation of the MSCs. On 2D substrates (Groups IV–VIII), the stiffer substrate was accompanied by a higher expression of Runx2 (Fig. 5A, red bars). The expression of osterix, type I collagen, ALKP and osteocalcin also indicated a similar effect of matrix stiffness (Fig. 5B–E, red bars). These results also demonstrated that increasing stiffness on 2D substrates promotes the osteogenic differentiation of MSCs.

Next, the gene expression profiles between 3D scaffolds and 2D substrates were compared. Comparing 3D scaffolds and 2D substrates of similar overall stiffness (i.e. Group I vs. Group IV, II vs. V, III vs. VI), the gene expression level of Runx2 was higher in 3D than in 2D on day 1 (Group III vs. VI), day 7 (Group II vs. V) and day 21 (Group I vs. IV, II vs. V). However, the expression of Runx2 showed no difference between Group III and VI on day 21 and the significantly decrease of Runx2 in Group III on day 21 also suggested osteoblast maturation (Fig. 5A). The expression of type I collagen was higher in 3D than in 2D on day 1 (Group II vs. V and III vs. VI), day 7 (Group II vs. V), day 14 (Group I vs. IV and

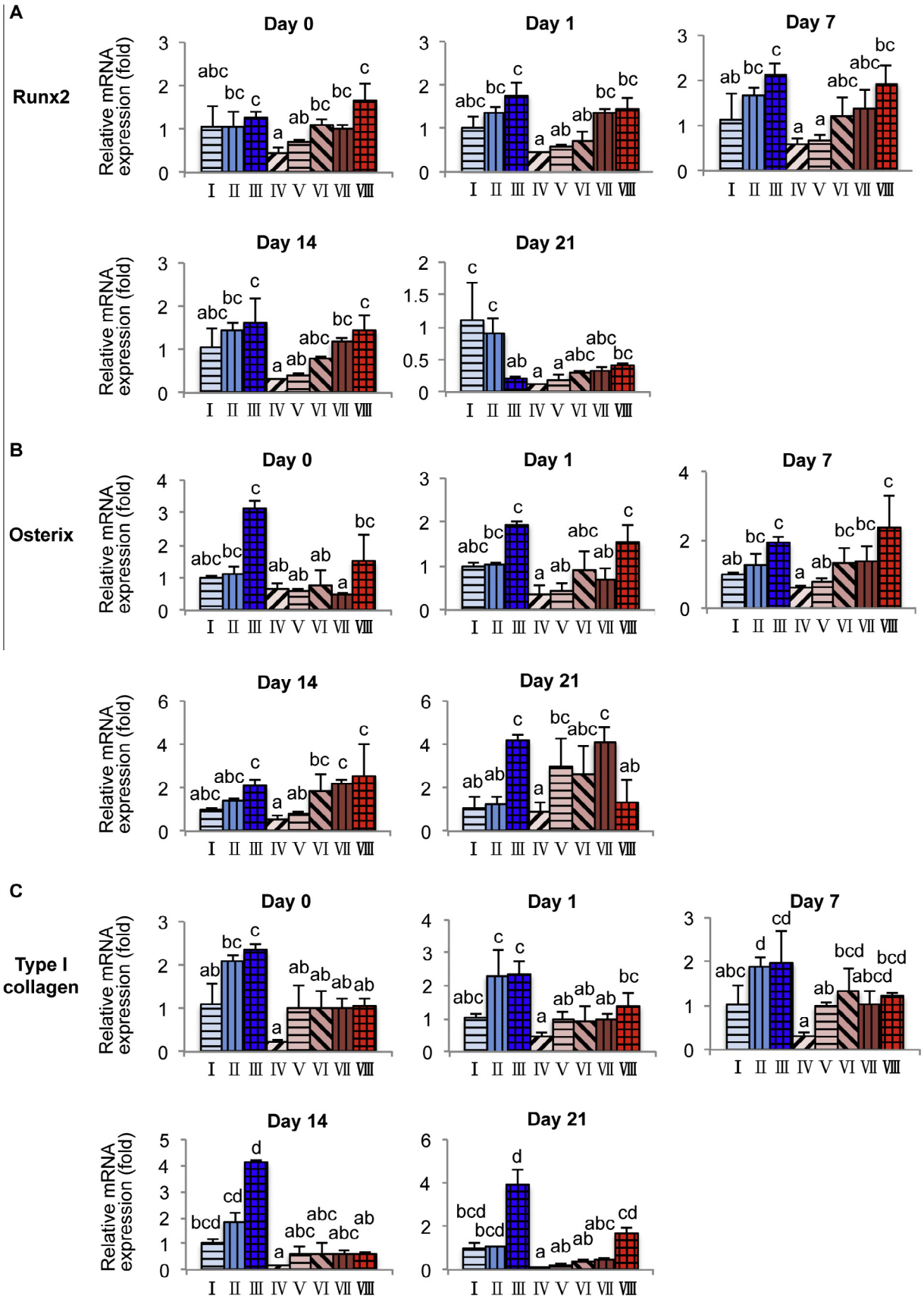

Fig. 5. Effect of matrix stiffness on MSCs between 3D and 2D microenvironment (A) relative gene expression on Runx2, (B) osterix, (C) type I collagen, (D) ALKP and (E) osteocalcin were compared between 3D scaffolds (Groups I–III) and 2D substrates (Groups IV–VIII) after inducing osteogenesis for 21 days. Statistical comparison was conducted between multiple groups by Kruskal–Wallis test followed by Dunn-Bonferroni post hoc test and groups with different letters represent statistical difference, $p < 0.05$. N.S = non significant. Data represented mean ± S.D., $n = 3$ (three independent experiments).

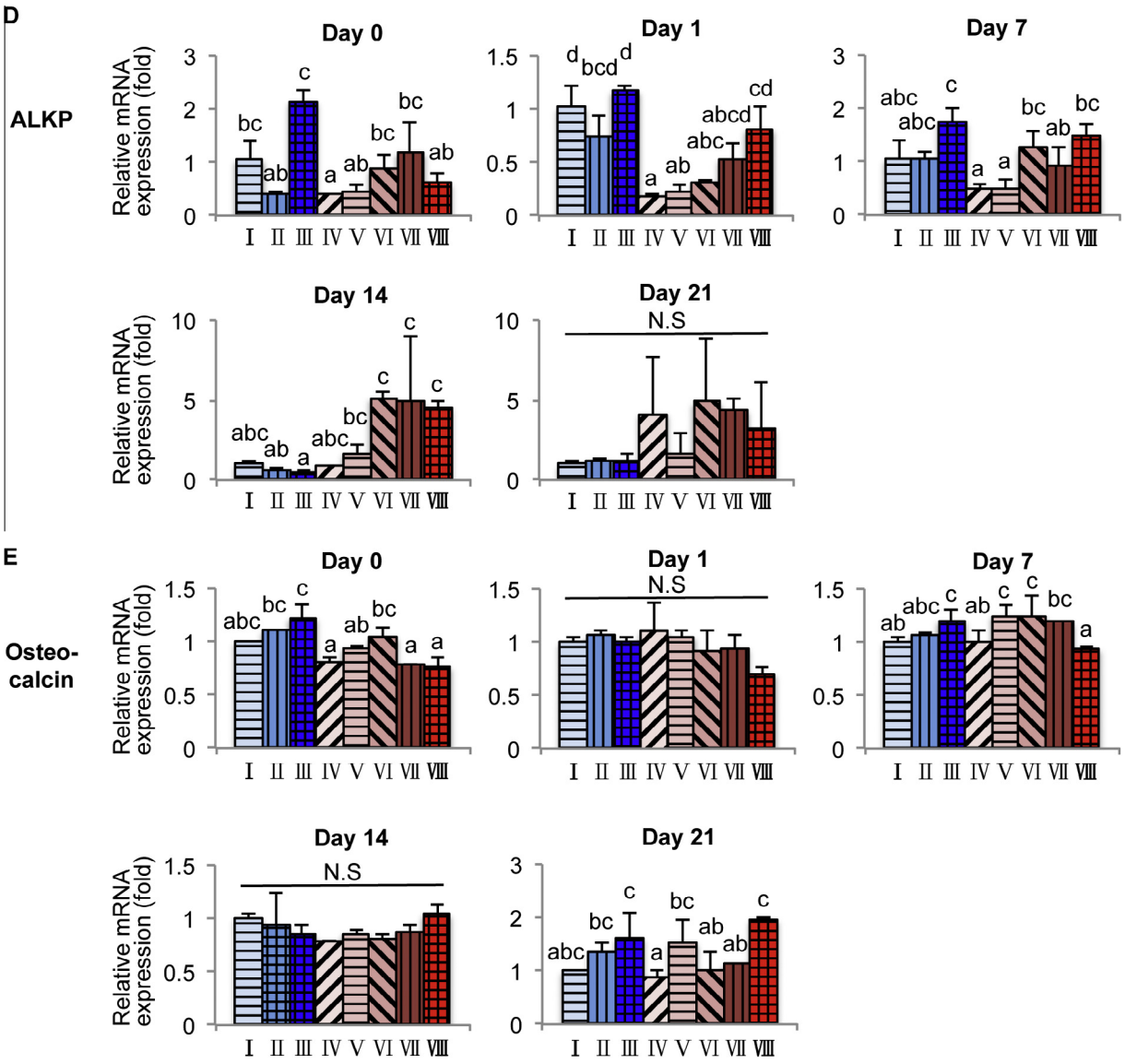

Fig. 5 (*continued*)

III vs. VI) and day 21 (Group I vs. IV and III vs. VI) (Fig. 5C). However, the expression of osterix showed no statistical difference at all times (Fig. 5B). The expression of ALKP was higher in 3D than 2D on days 1, but lower in 3D than 2D on days 14 (Group III vs. VI) (Fig. 5D). The earlier decreased expression of ALKP in 3D indicated that the maturation of osteoblasts occurred earlier in the 3D PA scaffolds. All the above results demonstrate that the 3D porous structure further promoted osteogenic differentiation of MSCs compared to the 2D flat structure. The gene expression levels of 3D scaffolds and 2D substrates composed of the same concentration of AC/BIS (i.e. Group I vs. V with a horizontal stripe pattern, II vs. VII with a vertical stripe pattern, and III vs. VIII with a grid pattern) were also compared. No statistical differences of Runx2 expression were found between 3D and 2D on days 1, 7 and 14. However, Runx2 expression in the Group I scaffolds was higher than the corresponding 2D hydrogels on day 21 (Fig. 5A). The results indicate the effect of dimensionality in the mature stage of osteogenesis. The type I collagen expression showed a trend similar to that for Runx2 on days 1 and 7. Moreover, the type I collagen expression in the 3D scaffolds was higher than the corresponding 2D hydrogels on days 14 and 21 (Fig. 5C). The ALKP expression in the 3D scaffolds was significant lower than the corresponding 2D hydrogel on day 14 (Group II vs. VII and III vs. VIII) (Fig. 5D). The results also support that the 3D porous structure promoted osteogenic differentiation of MSCs and the effect of dimensionality was observed in the mature stage of osteogenesis. Comparing all these eight groups, the expression level of Runx2 and osterix on days 1, 7 and 14 in Groups I–III were similar to Groups V, VII and VIII (Fig. 5A and B). The expression level of ALKP on days 1 and 7 showed similar trends (Fig. 5D). This implies that the influence of local stiffness of substrates on MSCs differentiation was higher than the overall stiffness.

3.5. Organization of F-actin in the 3D and 2D microenvironment

F-actin cytoskeleton plays a major role in the mechanotransduction for sensing and responding to extracellular physical stimuli [26]. Its structural organization is directly linked to external mechanical factors. For example, on a soft 2D substrate F-actins are often diffusive but on stiff 2D substrate they form thick stress fibers. It has been shown that the alignment of stress fibers of MSCs depends on matrix rigidity in 2D structures [27]. Here the

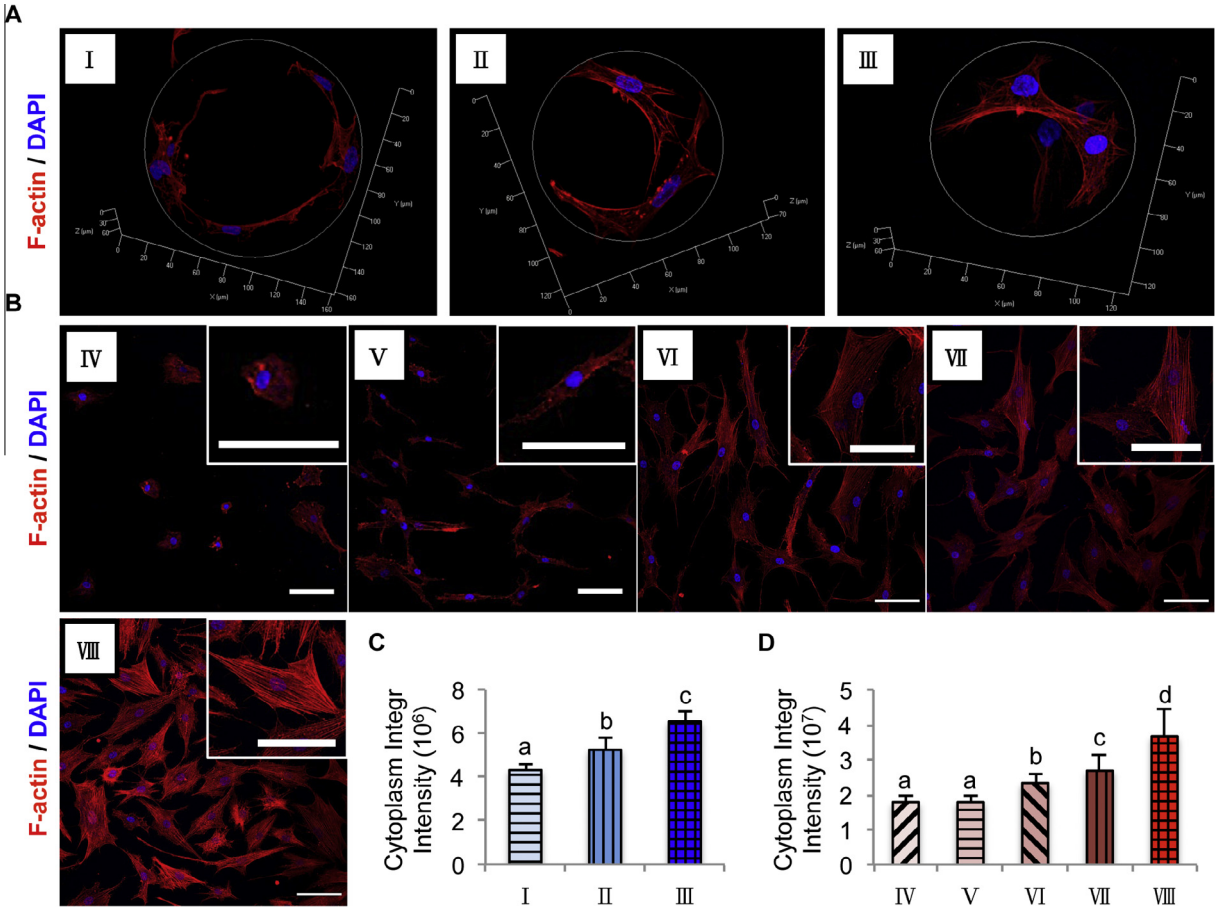

Fig. 6. Organization and quantification of F-actin in the 3D and 2D microenvironment (A) F-actin (rhodamine phalloidin, red) and nucleus (DAPI, blue) were co-stained on MSCs in the 3D PA scaffolds (Groups I–III) and (B) 2D PA hydrogels (Groups IV–VIII), scale bar = 100 μm. The immunofluorescence intensity of F-actin of a single MSC in (C) 3D scaffolds and (D) 2D hydrogels was quantified. Statistical comparison was conducted between multiple groups by one-way ANOVA followed by Tukey's post hoc test and groups with different letters represent statistical difference, $p < 0.05$. Data represented mean ± S.D., $n = 50$ (fifty cells).

organization of F-actin in 3D scaffolds one day after osteogenic induction was examined. The distribution of F-actin appeared more diffusive on both soft 3D scaffolds and 2D substrates but formed thick stress fibers on stiff 3D scaffolds and 2D substrates (Fig. 6A and B). The MSCs of Group I lay close to the wall and formed tortuous extensions along the wall (Fig. 6A). In Groups II and III, MSCs attached to the pore walls and spatially extended the cell bodies in all directions (Fig. 6A). As the stiffness of the 2D substrates increased, the morphology of MSCs was round, spindle-shaped and became flat, polygonal-shaped and pronounced actin stress fibers across the cell body were clearly observed (Fig. 6B). Both in 3D and 2D substrates, the average cytoplasmic fluorescence intensity of F-actin on stiffer groups was significantly higher than the softer ones and showed more parallel bundles (Fig. 6C and D). These results demonstrated that the organization of F-actin was correlated with matrix stiffness in 3D and this organization may promote osteogenesis.

4. Discussion

It has been shown that the stiffness of 2D substrates affects the physiological processes of MSCs such as morphology, proliferation, adhesion, migration and differentiation through F-actin organization [7,13,14,28]. The effect of matrix stiffness in 3D cultures requires additional study because the dimensionality also affects the F-actin distribution and, in addition to the factor of dimensionality, a 3D culture matrix often changes other factors such as permeability and nano-scale structure. A novel 3D cell culture scaffold is used, which differs from the conventional 2D compliant substrate mainly in terms of the substrate curvature. Our results can be directly compared with the 2D results to show the effect of 3D and 3D matrix stiffness.

Previous studies have shown that MSCs on soft PA hydrogels (1 kPa) had lower proliferation rates than those on stiff PA hydrogels (15 kPa) [28]. Pek et al. demonstrated that MSCs proliferated more rapidly in 3D matrices containing immobilized RGD, especially for the stiffer gels (>75 Pa) [11]. However, the result of cell proliferation assay in our study demonstrates that MSCs possess similar proliferation rates regardless of 3D matrix stiffness up to 21 days (Fig. 2D). This may be due to increased cell-cell interaction in 3D porous scaffolds than in 2D and 3D hydrogels, which also affects cell proliferation. The proliferation rate of MSCs in the 3D PA scaffolds increased over time, suggesting that PA scaffold is a suitable culture platform for the growth of MSCs. Moreover, the physical factors for cells are often not independent from their biochemical factors, but rather exhibit some interplay. For example, extracellular matrix (ECM) proteins could exert significant influence in determining the fate of MSCs [29]. In this study, fibronectin was used to coat the 3D PA scaffold for MSCs to attach to. The changeable surface coating during the manufacturing process of the 3D porous PA scaffold offers a platform to study the effect of different ECM proteins on the cell fate commitment of MSCs.

In 2D, Engler et al. demonstrated that matrix stiffness determined different lineage commitment of MSCs [7]. However, the phenomenon in 3D remains poorly investigated. We, for the first time, provided the direct evidence to demonstrate that in 3D scaffolds, matrix stiffness regulated the differentiation potential of MSCs, yet it did not alter the proliferation rates. Even though the effects of 3D hydrogel on osteogenic differentiation have been studied before [10–12], the biomechanical properties of 3D hydrogel are still distinct from those of 3D porous PA scaffolds. Using scaffolds of different architecture provides perspective from a different angle on 3D culture, which is important due to the diverse nature of 3D cell culture. For mechanically comparing the stiffness of PA scaffolds to actual bone, simple relation exists between two elastic constants ($E = 2G(1 + \upsilon)$, where E represents Young's modulus, G represents shear modulus, and υ represents Poisson's ratio) [30] in homogeneous material. The Poisson's ratio of polyacrylamide gel is 0.457 [31]. It has been reported that the modulus of elasticity of trabecular bone is 0.441–0.445 GPa [32,33]. Therefore, the stiffness of PA porous scaffolds ($G'_{scaffold}$ of Group III = 12 kPa) and hygrogels (G'_{gel} of Group VI = 11 kPa) is physiologically close to the bone precursor osteoid ($E_{osteoid} \sim 27 \pm 10$ kPa) [7], but not trabecular bone. In this study, the PA porous scaffold showed that high stiffness in 3D and 2D ($G'_{scaffold}$ = 12 kPa, G'_{gel} = 121 kPa) is preferred for osteogenesis. It also showed that at high stiffness the osteogenetic potential in the 3D scaffold is higher than in the 2D substrate. The results provide strong evidence that dimensionality plays an important role in determining stem cell fate. Furthermore, it was found that the biochemical expression of MSCs in the 3D scaffold is closer to that in the 2D substrate with the same AC/BIS concentration. This implies that MSCs sense the stiffness of the base material rather than the overall structural stiffness of a porous scaffold. Our study gains important insight on the effect of the base material in the porous scaffold.

The arrangement of the actin cytoskeleton is crucial in the osteogenesis of MSCs. Disruption of the actin cytoskeleton by cytochalasin-D decreases the osteogenesis and increases the adipogenesis of MSCs [34,35]. Moreover, matrix stiffness modulates the abundance and organization of actin stress fibers. Fibroblasts are plated on a stiff (2 MPa) substrate and display thicker and well-aligned stress fibers. In contrast, cells display thinner and poorly oriented stress fibers when plating on a soft (5 kPa) substrate [36]. Highly polarized stress-fibers in stem cells are important for stem cell differentiation [27]. It was also found that this condition also holds in 3D scaffolds. It is speculated that the ordered porous structure may facilitate F-actin organization when more cell–cell contacts form across the pores. Taken together, the 3D PA scaffold is a promising culture platform and our findings provide several insights for the physiology of MSCs in the 3D microenvironment.

The 3D culture systems mimic *in vivo* microenvironments with some limitations. Conventional 3D cultures often suffer from a tradeoff between nutrition and waste. Our scaffolds can be incorporated with microfluidic devices to serve as a micro-reactor [37] to optimize tissue engineering. In addition to physical cues, biochemical factors, such as TGF-β and BMP-2 also affect stem cell fate [28,38]. These previous findings encourage us to improve the culture condition in 3D scaffolds to promote differentiation of MSCs, or identify different mechanisms in 2D and 3D cultures by combining them with other biochemical signals. In a recent study, MSCs were encapsulated within covalently cross-linked hyaluronic acid (HA) hydrogels with MMP-degradable peptides. The result suggested that cell-mediated traction forces are important in determining the cytoskeletal assemblies and the fate of MSCs [39]. The stiffness-dependent arrangement and expression of F-actin of MSCs and the deformation of scaffolds with lower stiffness in this study implies that the tension force generated by MSCs plays an important role in differentiation and proliferation. In the future, the molecular mechanism of F-actin distribution and osteogenic potentials of MSCs in 3D scaffolds warrant further investigation. Polyacrylamide gel is a stable, non-toxic and non-resorbable material and its widely usage in breast reconstruction show the biocompatibility of the material [40–42]. Implanting the PA scaffolds into bone defect animals for bone regeneration is possible for advanced therapeutic application.

5. Conclusion

This study investigated the effects of the matrix moduli of 3D scaffolds and 2D substrates on the osteogenic differentiation of MSCs. It was found that cells cultured in 3D scaffolds show higher osteogenic differentiation than cells on the 2D flat substrates, and cells cultured with higher matrix stiffness show higher osteogenic differentiation. Furthermore, the MSC response to the matrix stiffness in 3D scaffolds is closer to the MSC response in 2D substrates made of the same base materials. This observation suggests that for tissue engineering purposes, one should consider the modulus of the scaffold base material. At higher matrix moduli in both 2D and 3D, there are more F-actin cytoskeletons and their organization are more bundled. The F-actin organization is favored for osteogenic differentiation. Collectively, MSCs respond differently to PA scaffolds with different mechanical moduli by adapting their morphology and distribution of F-actin that may affect its osteogenic potential. 3D PA scaffolds with the same geometric architecture and pore size and tunable mechanical properties are shown to be valuable for future studies of cellular mechanobiology and bone tissue engineering.

Disclosure of potential conflicts of interest

All authors have no potential conflict of interest to declare.

Acknowledgement

This work was supported in part by the UST-UCSD International Center of Excellence in Advanced Bio-engineering (Grant Number: MOST103-2911-I-009-101), under the Taiwan Ministry of Science and Technology I-RiCE Program. The authors acknowledge financial support from the Ministry of Science and Technology, Taiwan (MOST103-2314-B-010-053-MY3, MOST103-2120-M-010-001, MOST104-2321-B-010-008 and MOST105-2911-I-010-506). This study was also supported by Aiming for the Top University Plan, a grant from Ministry of Education and by the Academia Sinica Research Program on Nanoscience and Nanotechnology. The authors also acknowledge the technical support provided by Electron Microscopy Facility of National Yang Ming University and the Imaging Core Facility of Nanotechnology of the UST-YMU.

Appendix A. Supplementary data

Supplementary data associated with this article can be found, in the online version, at http://dx.doi.org/10.1016/j.actbio.2016.01.010.

References

[1] S.F. Badylak, Regenerative medicine and developmental biology: the role of the extracellular matrix, Anatomical Record B New Anatomist 287 (2005) 36–41.
[2] R.O. Hynes, The extracellular matrix: not just pretty fibrils, Science 326 (2009) 1216–1219.
[3] H. Krahl, U. Michaelis, H.G. Pieper, G. Quack, M. Montag, Stimulation of bone growth through sports. A radiologic investigation of the upper extremities in professional tennis players, Am. J. Sports Med. 22 (1994) 751–757.

[4] I.L. Weissman, Stem cells: units of development, units of regeneration, and units in evolution, Cell 100 (2000) 157–168.
[5] K. Matsuo, N. Irie, Osteoclast-osteoblast communication, Arch. Biochem. Biophys. 473 (2008) 201–209.
[6] R.G. Breuls, T.U. Jiya, T.H. Smit, Scaffold stiffness influences cell behavior: opportunities for skeletal tissue engineering, Open Orthopaedics J. 2 (2008) 103–109.
[7] A.J. Engler, S. Sen, H.L. Sweeney, D.E. Discher, Matrix elasticity directs stem cell lineage specification, Cell 126 (2006) 677–689.
[8] Y.R. Shih, K.F. Tseng, H.Y. Lai, C.H. Lin, O.K. Lee, Matrix stiffness regulation of integrin-mediated mechanotransduction during osteogenic differentiation of human mesenchymal stem cells, J. Bone Miner. Res. 26 (2011) 730–738.
[9] S. Dupont, L. Morsut, M. Aragona, E. Enzo, S. Giulitti, M. Cordenonsi, et al., Role of YAP/TAZ in mechanotransduction, Nature 474 (2011) 179–183.
[10] N. Huebsch, P.R. Arany, A.S. Mao, D. Shvartsman, O.A. Ali, S.A. Bencherif, et al., Harnessing traction-mediated manipulation of the cell/matrix interface to control stem-cell fate, Nat. Mater. 9 (2010) 518–526.
[11] Y.S. Pek, A.C. Wan, J.Y. Ying, The effect of matrix stiffness on mesenchymal stem cell differentiation in a 3D thixotropic gel, Biomaterials 31 (2010) 385–391.
[12] L.S. Wang, J. Boulaire, P.P. Chan, J.E. Chung, M. Kurisawa, The role of stiffness of gelatin-hydroxyphenylpropionic acid hydrogels formed by enzyme-mediated crosslinking on the differentiation of human mesenchymal stem cell, Biomaterials 31 (2010) 8608–8616.
[13] S.Y. Tee, J. Fu, C.S. Chen, P.A. Janmey, Cell shape and substrate rigidity both regulate cell stiffness, Biophys. J. 100 (2011) L25–7.
[14] J.R. Tse, A.J. Engler, Stiffness gradients mimicking in vivo tissue variation regulate mesenchymal stem cell fate, PloS One 6 (2011) e15978.
[15] Y.H. Lee, J.R. Huang, Y.K. Wang, K.H. Lin, Three-dimensional fibroblast morphology on compliant substrates of controlled negative curvature, Integr. Biol. 5 (2013) 1447–1455.
[16] T.M. Keaveny, E.F. Morgan, G.L. Niebur, O.C. Yeh, Biomechanics of trabecular bone, Annu. Rev. Biomed. Eng. 3 (2001) 307–333.
[17] T. Takebe, M. Enomura, E. Yoshizawa, M. Kimura, H. Koike, Y. Ueno, et al., Vascularized and complex organ buds from diverse tissues via mesenchymal cell-driven condensation, Cell Stem Cell 16 (2015) 556–565.
[18] T. Komori, Regulation of osteoblast differentiation by transcription factors, J. Cell. Biochem. 99 (2006) 1233–1239.
[19] P. Ducy, R. Zhang, V. Geoffroy, A.L. Ridall, G. Karsenty, Osf2/Cbfa1: a transcriptional activator of osteoblast differentiation, Cell 89 (1997) 747–754.
[20] K. Nakashima, X. Zhou, G. Kunkel, Z. Zhang, J.M. Deng, R.R. Behringer, et al., The novel zinc finger-containing transcription factor osterix is required for osteoblast differentiation and bone formation, Cell 108 (2002) 17–29.
[21] Y. Nishio, Y. Dong, M. Paris, R.J. O'Keefe, E.M. Schwarz, H. Drissi, Runx2-mediated regulation of the zinc finger Osterix/Sp7 gene, Gene 372 (2006) 62–70.
[22] M. Sandberg, H. Autio-Harmainen, E. Vuorio, Localization of the expression of types I, III, and IV collagen, TGF-beta 1 and c-fos genes in developing human calvarial bones, Dev. Biol. 130 (1988) 324–334.
[23] J.L. Frendo, G. Xiao, S. Fuchs, R.T. Franceschi, G. Karsenty, P. Ducy, Functional hierarchy between two OSE2 elements in the control of osteocalcin gene expression in vivo, J. Biol. Chem. 273 (1998) 30509–30516.
[24] Z. Huang, E.R. Nelson, R.L. Smith, S.B. Goodman, The sequential expression profiles of growth factors from osteoprogenitors [correction of osteroprogenitors] to osteoblasts in vitro, Tissue Eng. 13 (2007) 2311–2320.
[25] M. Fakhry, E. Hamade, B. Badran, R. Buchet, D. Magne, Molecular mechanisms of mesenchymal stem cell differentiation towards osteoblasts, World J. Stem Cells 5 (2013) 136–148.
[26] D.E. Ingber, Cellular mechanotransduction: putting all the pieces together again, FASEB J. 20 (2006) 811–827.
[27] A. Zemel, F. Rehfeldt, A.E. Brown, D.E. Discher, S.A. Safran, Optimal matrix rigidity for stress fiber polarization in stem cells, Nat. Phys. 6 (2010) 468–473.
[28] J.S. Park, J.S. Chu, A.D. Tsou, R. Diop, Z. Tang, A. Wang, et al., The effect of matrix stiffness on the differentiation of mesenchymal stem cells in response to TGF-beta, Biomaterials 32 (2011) 3921–3930.
[29] A.S. Rowlands, P.A. George, J.J. Cooper-White, Directing osteogenic and myogenic differentiation of MSCs: interplay of stiffness and adhesive ligand presentation, Am. J. Physiol. Cell Physiol. 295 (2008). C1037-44.
[30] I.S. Sokolnikoff, Mathematical Theory of Elasticity, second ed., Krieger Pub Co, Malabar, FL, 1983.
[31] T. Takigawa, Y. Morino, K. Urayama, T. Masuda, Poisson's ratio of polyacrylamide (PAAm) gels, Polym. Gels Networks 4 (1996) 1–5.
[32] A. Rohlmann, H. Zilch, G. Bergmann, R. Kolbel, Material properties of femoral cancellous bone in axial loading. Part I: time independent properties, Arch. Orthop. Trauma. Surg. 97 (1980) 95–102.
[33] F. Linde, I. Hvid, The effect of constraint on the mechanical behaviour of trabecular bone specimens, J. Biomech. 22 (1989) 485–490.
[34] R. McBeath, D.M. Pirone, C.M. Nelson, K. Bhadriraju, C.S. Chen, Cell shape, cytoskeletal tension, and RhoA regulate stem cell lineage commitment, Dev. Cell 6 (2004) 483–495.
[35] J.P. Rodriguez, M. Gonzalez, S. Rios, V. Cambiazo, Cytoskeletal organization of human mesenchymal stem cells (MSC) changes during their osteogenic differentiation, J. Cell. Biochem. 93 (2004) 721–731.
[36] M. Prager-Khoutorsky, A. Lichtenstein, R. Krishnan, K. Rajendran, A. Mayo, Z. Kam, et al., Fibroblast polarization is a matrix-rigidity-dependent process controlled by focal adhesion mechanosensing, Nat. Cell Biol. 13 (2011) 1457–1465.
[37] Y.S. Sun, S.W. Peng, K.H. Lin, J.Y. Cheng, Electrotaxis of lung cancer cells in ordered three-dimensional scaffolds, Biomicrofluidics 6 (2012) 14102–1410214.
[38] S. Tan, J.Y. Fang, Z. Yang, M.E. Nimni, B. Han, The synergetic effect of hydrogel stiffness and growth factor on osteogenic differentiation, Biomaterials 35 (2014) 5294–5306.
[39] S. Khetan, M. Guvendiren, W.R. Legant, D.M. Cohen, C.S. Chen, J.A. Burdick, Degradation-mediated cellular traction directs stem cell fate in covalently crosslinked three-dimensional hydrogels, Nat. Mater. 12 (2013) 458–465.
[40] L.H. Christensen, V.B. Breiting, A. Aasted, A. Jorgensen, I. Kebuladze, Long-term effects of polyacrylamide hydrogel on human breast tissue, Plast. Reconstr. Surg. 111 (2003) 1883–1890.
[41] Y. Zhao, Q. Qiao, Y. Yue, X. Kou, Z. Liu, Clinical and histologic evaluation of a new injectable implant: hydrophilic polyacrylamide gel, Ann. Plast. Surg. 53 (2004) 267–272.
[42] G. Patlazhan, D. Unukovych, K. Pshenisnov, Breast reconstruction and treatment algorithm for patients with complications after polyacrylamide gel injections: a 10-year experience, Aesthetic Plast. Surg. 37 (2013) 312–320.